BIW10 Preprint -- Edited; preliminary green dot status
Final version will appear on JACoW

BEAM HALO IMAGING USING AN ADAPTIVE OPTICAL MASK*

H. D. Zhang, R. B. Fiorito#, A. G. Shkvarunets, S. Bernal, I. Haber, R. A. Kishek, P. G. O'Shea,
University of Maryland, College Park, MD, USA
S. Artikova, MPI- Heidelberg, Heidelberg, Germany
C. Welsch, Cockcroft Institute, University of Liverpool, Liverpool, UK

Abstract

We have developed a technique that employs a digital micro-mirror array to produce an image of the halo of an electron beam with an enhanced dynamic range. Light produced by the beam intercepting a phosphor screen is first imaged onto the array; an adaptive mask is created and applied to filter out the beam core; and the result is reimaged onto an intensified CCD camera. We describe the optics used, the masking operation and preliminary results of experiments we have performed to study beam halo at the University of Maryland Electron Ring.

INTRODUCTION

Beam halo in intense beams is a phenomenon typically caused by parametric resonances or nonlinear forces due to space charge. It can lead to a number of undesirable effects, such as nuclear activation, emission of secondary electrons, and increased noise in the detectors. For high average power machines, halos can be damaging even if the number of particles in the halo is orders of magnitude below that in the core of the beam [1].

Halo can be observed by imaging visible light emitted by beam particles interacting with various types of screens, e.g. phosphor, YAG, OTR; or with optical synchrotron or edge radiation. However, there is usually an extreme contrast between beam core and halo; the ratio of halo to core intensity can be 10^{-5} or less. Therefore, a high dynamic range imaging system is required to view the details of the halo distribution. Also in any real optical system diffraction and scattering in the lenses due to the high core intensity can contaminate the halo image observed.

To solve these problems, several approaches have been considered. One is to allow the core intensity to saturate the camera. However, with sensitive CCD's and especially intensified CCD's, blooming and possible damage problems exist. Other methods are: passive spatial filtering, e.g. coronagraphy [2]; use of a high dynamic range (28 bit) camera such as the Spectra-Cam CID [3]: and, recently [4], an mask technique based on a digital micro-mirror array (DMA).

The DMA method has the advantages that the mask is adaptive to any shape beam and that a high dynamic range (DR) is achievable with a low cost camera; a DR~10^5 has been previously measured with a laser and a standard 8 bit CCD camera [4]. However, it has also been observed that the DMA produces a cross like diffraction pattern when illuminated by the laser; i.e. the DMA acts like a 2D grating. Since this may have a negative effect in an actual optical system used to image the beam, it is important to test the DMA in such a system.

We have developed an imaging method using a DMA to measure the halo of the electron beam at the University of Maryland Electron Ring (UMER) [5]. UMER is suitable machine to do halo experiments and test the theory of halo formation in space charge dominated beams. The beam is low energy (10 keV) but high current (10's of mA) with a variable pulse length (20-100 ns) and repetition rate (20-60 Hz). Radiation exposure is of minimal concern so that experiments can be easily set up and run *in situ*. Moreover, the beam is quite reproducible and stable over long time periods (hrs).

In the following sections, we will describe the optics system we have developed to image the beam with a DMA, the algorithm to spatially filter the image of the beam, our measurements of the dynamic range and optical performance of the system and finally preliminary beam halo images obtained with an adaptive mask.

EXPERIMENT SETUP

Digital micro-mirror array

The DMA we use is the DMD Discovery 1100 manufactured by Texas Instruments Inc. [6]. This type of device which is widely used in projectors and digital TV's is made up of hundreds of thousands of microscopic mirrors. A segment of the array and a mechanical drawing of one element are shown in Fig. 1(a) and 1(b) [6]. Each mirror on the chip can be individually addressed and rotated to either $+12^\circ$ or -12° with respect to the normal, when a voltage is applied to electrodes situated underneath the corners of each micro-mirror. When the voltage to the DMA is zero, all the mirrors are in a nominally flat, floating state.

Light from an external source can be reflected from mirrors in one state, e.g. $+12^0$, along a desired optical path, while the light reflected by mirrors in the opposite (-12^0) state will be directed 48^0 away from this optical path. When incorporated into an imaging system the device can be used as a spatial light modulator. The parameters of the device are shown in Table 1 [6].

*Work supported by the US Office of Naval Research, the Joint Technology Office and the US Department of Energy.
#rfiorito@umd.edu

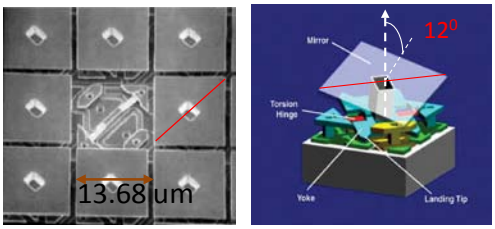

(a) (b)

Figure 1: (a) segment of the DMA; (b) mechanical drawing of individual micro-mirror and substructure .

Table 1: DMD Discovery 1100 Parameters

Parameter	Value
Mirror size	13.68 μm x 13.68 μm
switching rate	9,600 frames/s
PC interface	USB 2.0
Resolution	1024 x 768 pixels

Optical system

The basic layout of our optical imaging system is presented in Fig. 2 which shows a test bench setup. The optics implemented on UMER is essentially the same except the target screen in the real experiment is replaced by a phosphor screen.

Two lenses seen in the lower part of Fig. 2 are used to adjust the magnification and to focus the target onto the surface of the DMA, which is normal to the axis, when the device is in the floating state. When all mirrors switched to the $+12^0$ (or +) state, the image of the target is directed into a second optical channel (top part of Fig. 2) and refocused onto a 16 bit, gated, intensified, cooled CCD (PIMAX2). Since the rotation axis of the micro-mirrors is not parallel to the vertical or horizontal direction of the array, which corresponds to the sides of a micro-mirror, but rather along the diagonal of the later, the DMA must be rotated by 45^0, as shown in Fig. 3(a), to maintain the optical axis in the horizontal plane.

The two lenses used in the second channel control the magnification and focus of the image onto the CCD. Note that the camera is tilted horizontally by 24^0 with respect to the optical axis to compensate for the depth focusing problem produced by the $+12^0$ tilt angle of the micro mirrors. This angle produces differences in the path lengths of the rays which emanate from different horizontal source points on the DMA. This method is commonly used in photography and is known as Scheimflug compensation [7].

The position and tilt angle of the camera are adjusted to achieve a clear undistorted image of the target and the DMA itself as shown in Fig. 3(b). The target we use is a

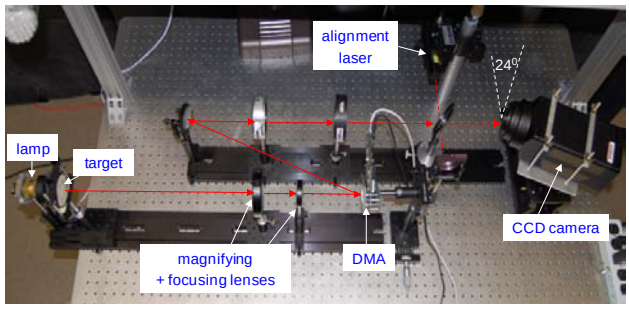

Figure 2: Optical imaging system incorporating the DMA.

semi-transparent rectangular grid overlaid with a circle with a diameter of 32 mm, the same size as the phosphor screens used to image the beam.

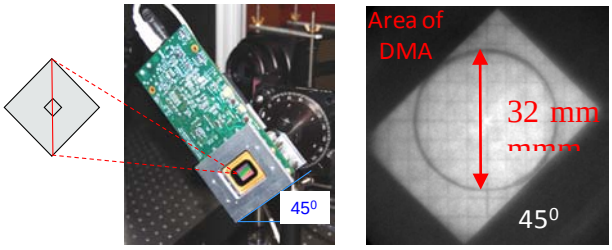

(a) (b)

Figure 3: (a) DMA device rotated by 45^0 and resulting orientation of a single micro-mirror; (b) image of the test target on the ICCD with Scheimflug compensation.

Algorithm for mask generation

Because of the 45^0 orientation of DMA and the differences in the number of pixels between the CCD and the DMA, we need to do a coordinate transformation and rescaling before we can generate an optical mask on the DMA. The algorithm shown schematically in Fig. 4 is described as follows.

First we take a calibration picture in order to observe the edges of the DMA on the camera and consequently to determine the size of DMA (Δx, Δy) in units of camera pixels. Any point of interest (x_0, y_0), can then be transformed to the DMA coordinates by calculating the distance between the point and the edges of the DMA. Next linearly magnify the image on the DMA originally given in units of camera pixels to its size in DMA pixels.

We then choose selected points on the beam image as a first step in generating a mask. For example, we can use points in the 'core' of the beam as the selected points, by (1) specifying a particular geometric area (e.g. a circular disk) overlaid on the 'core' visually, or (2) setting an intensity threshold to define the 'core'. Then we program the DMA, to blank out the 'core' pixels by setting them to -12^0 (see the red dot in Fig. 4). Finally, we reimage the beam with the mask set on the DMA.

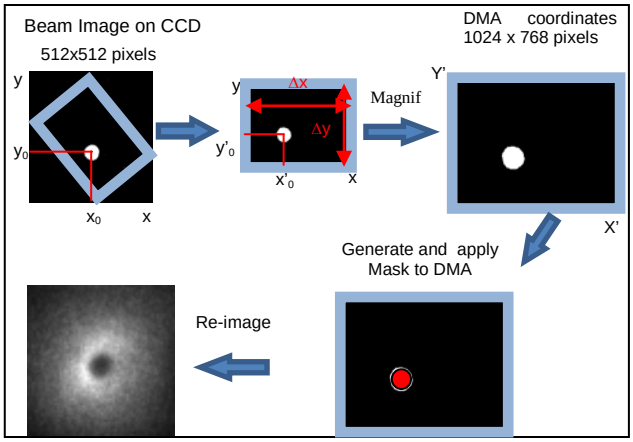

Figure 4: Schematic of mask generation algorithm.

RESULTS

Test of the Performance of the DMA

We first tested the effectiveness of the DMA to filter (reject) light from the phosphor screen by changing the DMA pixels from all ' + ' to all ' – '.When all the pixels of the DMA are '+', the light from the beam on the phosphor screen passes through the optics. We then integrate until the peak intensity approaches saturation on the CCD (64K counts); see Fig. 5(a). When all pixels are switched to '-', almost all of the light from the phosphor screen is reflected out of the optical path and only a very low level (~200 counts) from stray light scattered from the edges of the DMA is visible; see Fig. 5(b). Note the difference in the intensity scales between Fig. 5(a) and 5(b).

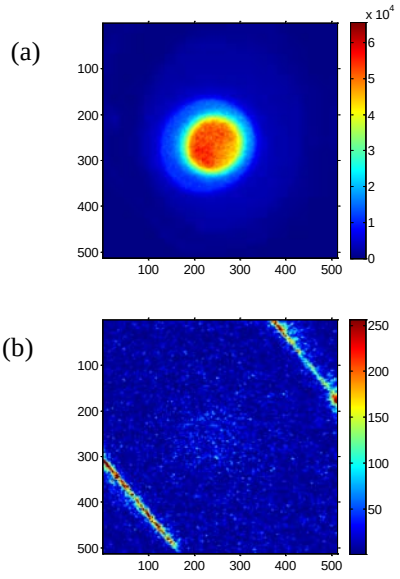

Figure 5: (a) Image with all DMA pixels set to $+12^0$; (b) image with all pixels set to -12^0; vertical and horizontal coordinates are given in terms of CCD pixels.

Next we did an experiment to test if the DMA affects the quality of the image. We compared images for three different cases using: 1) the DMA with all pixels set to '+' and Scheimflug compensation; 2) the DMA with all pixels in the floating state and no compensation; and 3) a simple mirror, which replaces the DMA and no compensation.

Fig. 6 shows the resulting beam images taken for each of these cases. Note that the optics must be slightly adjusted between configurations. This causes slight differences in the magnification and number of peak counts for each case. So we have normalized the intensities by the peak values in each image in order to concentrate on differences in the beam profile. No major differences are observed. We conclude that diffraction and scattering by the DMA mirrors has little if any effect on the quality of the beam images.

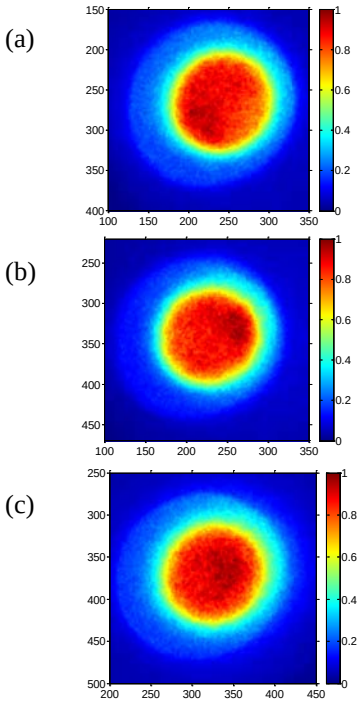

Figure 6: Comparison of beam images (close ups) with: (a) all DMA pixels set to '+' and Scheimflug compensation; (b) all DMA pixels floating and no compensation; (c) simple mirror and no compensation.

Dynamic Range Measurement

In order to determine the dynamic range of our optical system we observed an intense beam (I=23mA) focused to a 2.85 mm diameter on the phosphor screen, the minimum achievable size with our solenoid focusing magnet. We then generated a number of circular masks with different radii but a common origin, i.e. the position of the peak intensity of the beam observed without a mask.

For each mask we selected the appropriate number of gates on our ICCD camera necessary to bring the peak intensity in the image to near the saturation level of the camera. Note the small highlights visible in the upper left hand part of pictures in the second row. These are due to scattering of the phosphor light from a metal edge on the screen. We added a second small mask to block out these highlights which is seen as black dots on the lower images of Fig. 7.

To obtain a background image, we turned the beam off and integrated for the same number of gates used to obtain the beam image. Background subtracted images are shown in Fig. 7; the number below each picture is the number of gates used to obtain that particular image. By taking the horizontal line scans of all beam profiles (note for reference the horizontal red line in Fig. 7) and normalizing by the number of gates taken for each image, we can present the results as a series of plots as shown in Fig. 8. Each of the scans in the Fig. 8 corresponds to one of the pictures in Fig. 7. Note that the intensity fluctuations in tails of the beam profiles get smaller as more integration is applied. Moreover, the noise level outside the screen decreases to ~10^{-5}. Using the data presented in Fig. 7, and Fig. 8, we can reconstruct the 2D beam profile as shown in Fig. 9.

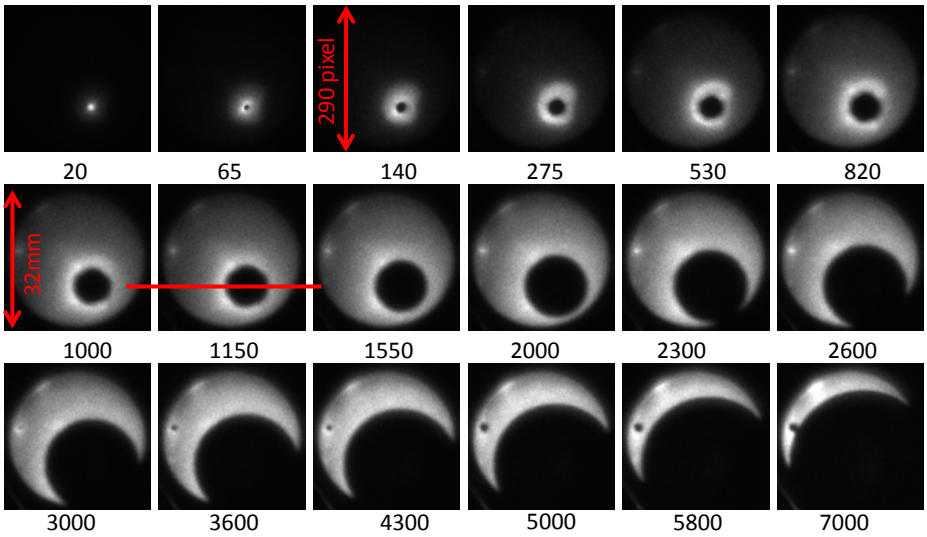

Figure 7: Images of the same beam with the DMA set to concentric circular mask of successively larger radii; number below image denotes the number of frame integrations on the ICCD camera.

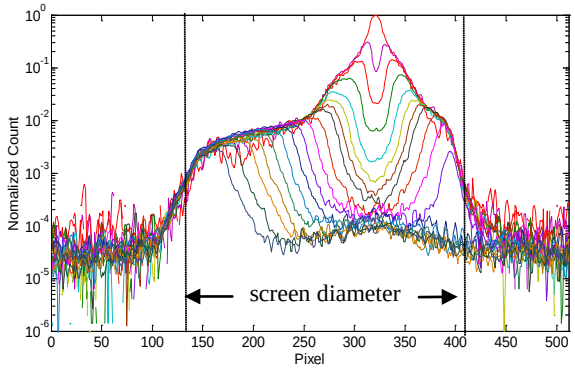

Figure 8: normalized horizontal scans of beam profiles presented in Fig. 7.

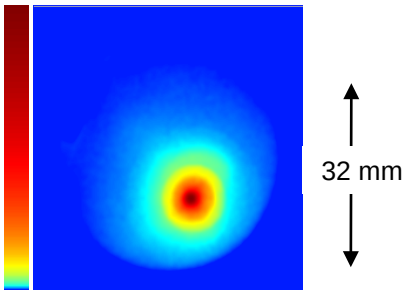

Figure 9: Reconstructed beam profile using color logarithmic intensity scale.

Halo imaging with an adaptive mask

Fig. 10 (a) shows a black and white image of the beam with halo that was previously presented above in Fig. 5. Note that neither the core nor the halo distributions are axisymmetric. However, by setting a threshold condition (e.g. 10^4 counts), we use the DMA to can create an adaptive optical mask to block out the 'core', i.e. all pixels in the beam image with intensity levels greater than a given value. As described above, we can then increase the number of gates to better view the halo distribution by

bringing the peak intensity of the halo close to saturation. The ratio of the number of frames integrated with the DMA mask (180) to those taken without the mask (900) is 5, which effectively increases the dynamic range of the measurement.

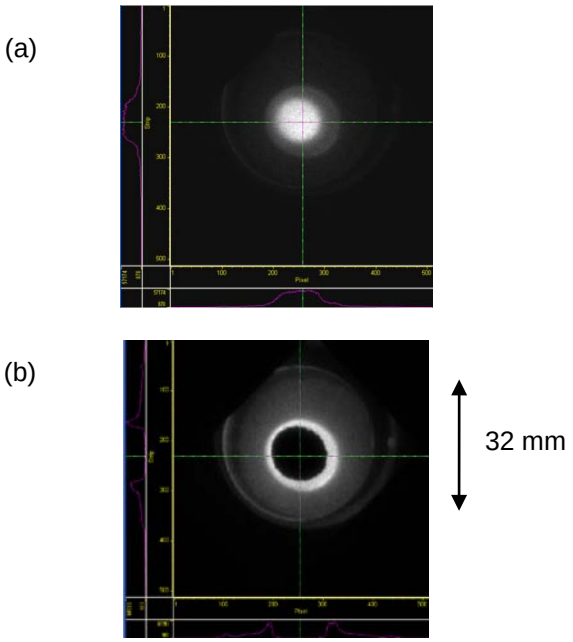

Figure 10: (a) Beam profile with core and halo; (b) profile of the halo after applying adaptive threshold mask with intensity level of 10^4 counts.

By lowering the threshold level and increasing the integration time, similar to what was done with the circular masks (see Fig. 7), we can view the tail of the halo distribution, up to the limit of the screen size, with a further increase in dynamic range.

CONCLUSIONS AND FUTURE WORK

We have developed a flexible optical system employing a DMA to adaptively mask the beam central core and image the halo with an improved dynamic range. We show that a dynamic range of close to 10^5 is achievable using the DMA to image and mask the UMER electron beam with a simple phosphor screen. This performance matches earlier measurements which used the DMA and a laser only. Furthermore, we have performed tests to show that the DMA has excellent extinction (~10^5) and that effects of diffraction and scattering due to the DMA on beam images are minimal.

Some features of UMER and the imaging screen used in our measurements, such as the highest beam intensity achievable, the efficiency of the phosphor, the ratio of the beam to the screen size, scattered light and background, limited our measured dynamic range. This limit may be exceeded at other machines which have a higher intensity beam and/or with improved optics.

We plan to study the halo evolution around the UMER ring using the DMA as well as apply our technique to a higher energy accelerator using other beam based emissions, e.g. OTR or optical edge radiation.

REFERENCES

[1] J. Wei, W. Fischer, P. Manning (eds.), Beam Halo Dynamics, Diagnostics and Collimation, Proc. of 29th ICFA Advanced Beam Dynamic Workshop, AIP Conf. Proc. 693, Melville, NY (2003).

[2] T. Mitsuhashi, "Design and construction of coronagraph for observation of beam halo", Proceedings of EPAC 2004, Lucerne, Switzerland (2004).

[3] C. P. Welsch, E. Bravin and T. Lefevre, "A beam halo monitor based on adaptive optics", Proc. SPIE 6616,9 (2007).

[4] J. Egberts, S. Artikova, C. P. Welsch, "Flexible core masking technique for beam halo measurements with high dynamic range", Proceedings of DIPAC09, Basel, Switzerland (2009).

[5] R. A. Kishek, et. al. 'The University of Maryland ele ctron ring (UMER) enters a new regime of high tune shift rings', Proc. of PAC 07, p. 820 (2007).

[6] Texas Instruments Inc., "DMD Discovery 1100 Controller Board and Starter Kit", 2005.

[7] T. Scheimflug, "Improved Method and Apparatus for the Systematic Alteration or Distortion of Plane Pictures and Images by Means of Lenses and Mirrors for Photography and for other purposes", GB Patent No. 1196. issued 12 May 1904; see also http://www.trenholm.org/hmmerk/#SR